JOURNAL OF SPACECRAFT AND ROCKETS
Vol. 45, No. 6, November–December 2008

Nonparallel Flow Effects on Roughness-Induced Perturbations in Boundary Layers

Anatoli Tumin*
University of Arizona, Tucson, Arizona 85721

DOI: 10.2514/1.37136

The nonparallel flow effects on roughness-induced perturbations in subsonic boundary layers over a flat plate are explored within the scope of the linearized Navier–Stokes equations. The receptivity problem is treated under the parallel flow approximation, and the nonparallel flow effects on the perturbations development are taken into account. The analysis is based on the method of multiple scales when intermodal exchange due to the nonparallel character of the flow is neglected. The nonparallel flow effects lead to lower velocity and higher temperature in the wake downstream from the hump.

Nomenclature

$\mathbf{A}$	=	perturbation function vector
$\mathbf{A}_{\alpha\beta}$	=	eigenfunction of the direct problem
a	=	height of the roughness element
$\mathbf{B}_{\alpha\beta}$	=	eigenfunction of the adjoint problem
F	=	frequency parameter, $\omega\mu_e/\rho_e U_e^2$
$f(x, z)$	=	shape of the roughness element
k	=	parameter of the continuous spectrum
$\mathbf{L}_j, \mathbf{H}_j$	=	16×16 matrices
L_z	=	spanwise period of the roughness-element array
l_x	=	streamwise length scale of the roughness element
l_z	=	spanwise length scale of the roughness element
M	=	Mach number
Pr	=	Prandtl number
Re	=	Reynolds number
T	=	temperature
t	=	time
U	=	streamwise velocity
u	=	streamwise velocity perturbation
V	=	vertical velocity
v	=	normal velocity perturbation
w	=	spanwise velocity perturbation
X	=	slow streamwise coordinate, ϵx
x	=	distance from the leading edge
x_0	=	distance from the leading edge to the roughness element
x_*	=	$x - x_0$
y	=	coordinate normal to the wall
z	=	spanwise coordinate
α	=	streamwise wave number
β	=	spanwise wave number
γ	=	specific heats ratio
Δk	=	width of the narrow-wave packet
ε	=	small parameter
η	=	distance from the wall scaled with $(\mu_e x/\rho_e U_e)^{1/2}$
θ	=	temperature perturbation
Λ	=	receptivity efficiency
μ	=	viscosity
π	=	pressure perturbation
ρ	=	density
φ	=	Fourier transform of the roughness shape
ω	=	angular frequency

Subscripts

ad	=	adiabatic wall condition
e	=	edge flow parameter
s	=	unperturbed boundary layer
w	=	wall parameter

Presented as Paper 0504 at the 46th AIAA Aerospace Sciences Meeting and Exhibit, Reno, NV, 6–10 January 2008; received 13 February 2008; revision received 21 July 2008; accepted for publication 1 August 2008.

*Professor, Department of Aerospace and Mechanical Engineering. Associate Fellow AIAA.

I. Introduction

IT HAS been observed in experiments that roughness elements can trigger early transition to turbulence in boundary layers. One of the possible scenarios is associated with the transient-growth mechanism: namely, that tiny roughness elements introduce transient perturbations that grow sufficiently to be responsible for the laminar–turbulent transition [1,2]. Theoretical studies have dealt mostly with optimal perturbations: those that lead to the largest energy growth at some downstream location. Extensive theoretical analyses of optimal disturbances in incompressible and compressible flows [3,4] led to correlations for transition Reynolds numbers that are consistent with the available experimental data [5] related to roughness-induced transition. From the theoretical studies, optimal transient growth is associated with streamwise vortices. To investigate the transient-growth mechanism experimentally, an array of roughness elements was used in [6,7]. Although the experimental results agree qualitatively with the theoretical results, there are quantitative differences. To resolve the discrepancy and to complete the transient-growth scenario, one has to solve the receptivity problem (i.e., find the flow perturbation generated by an array of humps).

Boundary-layer flows in the presence of three-dimensional humps have been investigated extensively with the help of asymptotic methods [8–12] in the limit $Re_L^{-1/8} \to 0$, where Re_L is the Reynolds number based on the characteristic length of the oncoming boundary layer L and the freestream velocity U_∞. The asymptotic methods are very helpful for an overall understanding of flow structure and for the purpose of deriving the governing parameters, whereas the quantitative results might be questionable at finite Reynolds numbers. Therefore, it would be preferable to solve the receptivity problem with the help of a method that is applicable to the case of finite Reynolds numbers.

The flow response to a small roughness element on the wall is a particular example of the general receptivity problem. Usually, the term *receptivity* is used for the generation of instability modes only. Because the method applied in the present work originated as a method for solving receptivity problems in boundary layers at finite

Reynolds numbers, we would like to outline its origin and how it was verified by comparison with other methods.

Morkovin [13] and Reshotko [14] clarified the important role of receptivity in the laminar–turbulent transition process. These papers motivated intensive investigations of various mechanisms responsible for excitation of unstable Tollmien–Schlichting (TS) waves. A partial listing of the vast bibliography on the topic is presented in [15–18].

Theoretical models may be categorized according to their underlying principles as follows: 1) the asymptotic analysis of the linearized Navier–Stokes equations at large Reynolds numbers ($Re_L \to \infty$) and 2) the finite-Reynolds-number approach based on a combination of analytical models with numerical representation of normal modes.

At large but finite Reynolds numbers, a method based on expansion of the solution into a biorthogonal eigenfunction system was introduced in [19–23]. The method turned out to be a powerful technique for solving receptivity problems for spatially developing perturbations. It was proven [24,25] that the receptivity solution based on the biorthogonal eigenfunction expansion is equivalent to the method used by Ashpis and Reshotko [26], whereas in the triple-deck limit, the method leads to the results by Smith et al. [8] and Terent'ev [27].

Recently, the biorthogonal eigenfunction system was applied to the problem of flow perturbation generated by a three-dimensional hump (an array of humps) placed on the wall [18,28]. The difference between the receptivity solution for TS waves and for roughness-induced perturbations is that the TS waves represent a discrete mode, whereas the roughness-induced perturbation is composed of an infinite number of modes belonging to continuous spectra (vorticity, entropy, and acoustic modes). The results in [18,28] were based on the parallel flow approximation. The nonparallel flow effects could have an effect on the receptivity itself and on the development of the perturbations on a length scale that is much larger than the boundary-layer thickness.

The nonparallel flow effects on receptivity are important when the source of the disturbances is distributed on a scale larger than the boundary-layer thickness. Choudhari [29] and Bertolotti [30] developed methods that can be used for analysis of the receptivity when the nonparallel flow effects are to be included. The nonparallel flow effects on the development of unstable discrete modes on a length scale that is much larger than the boundary-layer thickness have been studied within the scope of the method of multiple scales [31–39]. Another method that allows inclusion of the nonparallel flow effects on TS waves is based on the parabolized stability equations (PSE) [40–42]. To our knowledge, nonparallel flow effects on modes of the continuous spectra have not been addressed yet.

The objective of the present work is to develop a theoretical model for nonparallel flow effects in the case of perturbations associated with the continuous spectra and to analyze roughness-induced perturbations in subsonic boundary layers.

Briefly, the structure of the paper is as follows. The problem formulation is outlined in Sec. II. A theoretical model for roughness-induced perturbations, including the nonparallel flow effects, is presented in Sec. III. Numerical results for perturbations generated by an array of roughness elements ($M = 0.02$ and 0.5) are discussed in Sec. IV. In Sec. V, we formulate the main conclusions stemming from the results.

II. Governing Equations

We consider a compressible two-dimensional boundary layer in the Cartesian coordinates, where x and z are the downstream and spanwise coordinates, respectively, and coordinate y corresponds to the distance from the wall. We write the governing equations (the linearized Navier–Stokes equations) for a periodic-in-time perturbation (the frequency is equal to zero in the case of a roughness-induced perturbation), $\sim \exp(-i\omega t)$, in matrix form as

$$\frac{\partial}{\partial y}\left(\mathbf{L}_0 \frac{\partial \mathbf{A}}{\partial y}\right) + \mathbf{L}_1 \frac{\partial \mathbf{A}}{\partial y} = \mathbf{H}_1 \mathbf{A} + \mathbf{H}_2 \frac{\partial \mathbf{A}}{\partial x} + \mathbf{H}_3 \frac{\partial \mathbf{A}}{\partial z} + \mathbf{H}_4 \mathbf{A} \quad (1)$$

where vector $\mathbf{A}$ has 16 components,

$$\mathbf{A}(x, y, z) = (u, \partial u/\partial y, v, \pi, \theta, \partial\theta/\partial y, w, \partial w/\partial y, \partial u/\partial x, \times \partial v/\partial x, \partial\theta/\partial x, \partial w/\partial x, \partial u/\partial z, \partial v/\partial z, \partial\theta/\partial z, \partial w/\partial z)^T \quad (2)$$

$\mathbf{L}_0$, $\mathbf{L}_1$, $\mathbf{H}_1$, $\mathbf{H}_2$, $\mathbf{H}_3$, and $\mathbf{H}_4$ are 16×16 matrices (their definitions are given in the Appendix); u, v, w, π, and θ represent three velocity components, pressure, and temperature perturbations, respectively; and the superscript T in Eq. (2) stands for transposed. Matrix $\mathbf{H}_4$ originates from the nonparallel character of the flow. It includes terms with y component of the mean flow velocity and derivatives of the mean flow profiles with respect to the coordinate x. The second, fourth, and eighth equations of the system (1) are linearized x-, y-, and z-momentum equations, respectively; the third equation is the linearized continuity equation; and the sixth equation is the linearized energy equation. The other equations serve as definitions of the components (derivatives) in vector $\mathbf{A}$.

We use the Fourier transform with respect to the coordinate z:

$$\mathbf{A}_\beta(x, y) = \int_{-\infty}^{\infty} e^{-i\beta z} \mathbf{A}(x, y, z) \mathrm{d}z \quad (3)$$

In the quasi-parallel flow approximation, the solution of the linearized Navier–Stokes equations can be expanded into normal modes of the discrete and continuous spectra [43]:

$$\mathbf{A}_\beta(x, y) = \sum_\nu d_\nu A_{\alpha_\nu \beta}(y) e^{i\alpha_\nu x} + \sum_j \int_0^\infty d_j(k) A_{\alpha_j \beta}(y) e^{i\alpha_j(k)x} \mathrm{d}k \quad (4)$$

where Σ_ν and Σ_j denote sums over the discrete spectrum and branches of the continuous spectra, respectively. The coefficients d_ν and d_j are to be found from the receptivity problem solution [18].

The following biorthogonal eigenfunction system $\{\mathbf{A}_{\alpha\beta}, \mathbf{B}_{\alpha\beta}\}$ was formulated in [43]:

$$\frac{\mathrm{d}}{\mathrm{d}y}\left(\mathbf{L}_0 \frac{\mathrm{d}\mathbf{A}_{\alpha\beta}}{\mathrm{d}y}\right) + \mathbf{L}_1 \frac{\mathrm{d}\mathbf{A}_{\alpha\beta}}{\mathrm{d}y} = \mathbf{H}_1 \mathbf{A}_{\alpha\beta} + i\alpha \mathbf{H}_2 \mathbf{A}_{\alpha\beta} + i\beta \mathbf{H}_3 \mathbf{A}_{\alpha\beta}$$
$$y = 0\text{: } A_{\alpha\beta 1} = A_{\alpha\beta 3} = A_{\alpha\beta 5} = A_{\alpha\beta 7} = 0, \qquad y \to \infty\text{: } |A_{\alpha\beta j}| < \infty \quad (5)$$

$$\frac{\mathrm{d}}{\mathrm{d}y}\left(\mathbf{L}_0^T \frac{\mathrm{d}\mathbf{B}_{\alpha\beta}}{dy}\right) - \mathbf{L}_1^T \frac{\mathrm{d}\mathbf{B}_{\alpha\beta}}{dy} = \mathbf{H}_1^T \mathbf{B}_{\alpha\beta} + i\alpha \mathbf{H}_2^T \mathbf{B}_{\alpha\beta} + i\beta \mathbf{H}_3^T \mathbf{B}_{\alpha\beta}$$
$$y = 0\text{: } B_{\alpha\beta 2} = B_{\alpha\beta 4} = B_{\alpha\beta 6} = B_{\alpha\beta 8} = 0, \qquad y \to \infty\text{: } |B_{\alpha\beta j}| < \infty \quad (6)$$

Actually, Eq. (6) defines the complex conjugate of the conventional adjoint problem.

The eigenfunction system $\{\mathbf{A}_{\alpha\beta}, \mathbf{B}_{\alpha\beta}\}$ has an orthogonality relation given as

$$\langle \mathbf{H}_2 \mathbf{A}_{\alpha\beta}, \mathbf{B}_{\alpha'\beta} \rangle \equiv \int_0^\infty (\mathbf{H}_2 \mathbf{A}_{\alpha\beta}, \mathbf{B}_{\alpha'\beta}) \mathrm{d}y = \Gamma \Delta_{\alpha\alpha'} \quad (7)$$

where Γ is a normalization constant, $\Delta_{\alpha\alpha'}$ is a Kronecker delta if either α or α' belong to the discrete spectrum, and $\Delta_{\alpha\alpha'}$ is a Dirac delta function if both α and α' belong to the continuous spectrum. Because Eq. (6) represents the complex conjugate of the conventional problem, the dot product $(,)$ in Eq. (7) does not involve complex conjugation.

Solutions of linear Eqs. (5) and (6) depend on the choice of their normalization. In a parallel flow, one can choose any fixed normalization of the solutions. In the case of a weakly nonparallel flow, coefficients of Eqs. (5) and (6) are slow functions of the streamwise coordinate x, and there is uncertainty with the solutions' normalization (the solutions can be multiplied by a function of the coordinate x). Therefore, the normalization constant Γ in Eq. (7) can be a function of coordinate x, depending on normalization of the solutions $\{\mathbf{A}_{\alpha\beta}, \mathbf{B}_{\alpha\beta}\}$. However, for any normalization of $\mathbf{A}_{\alpha\beta}$, one

can make Γ be a constant by an appropriate choice of $\mathbf{B}_{\alpha\beta}$. In the present work, the final result leads to a solution independent of the particular normalizations of $\{\mathbf{A}_{\alpha\beta}, \mathbf{B}_{\alpha\beta}\}$, and one may choose it based on consideration of convenience.

III. Weakly Nonparallel Flow Analysis

A. Discrete Mode

For the purpose of clarity, we begin with an outline of an analysis for a discrete mode in a weakly nonparallel boundary layer (see, for example, [37]). In a weakly nonparallel flow, one can employ the method of multiple scales by introducing fast (x) and slow ($X = \varepsilon x$ and $\varepsilon \ll 1$) scales. The mean flow profiles depend on y and X only, whereas the perturbation will depend on both length scales. In the case of a discrete mode, solution of the linearized Navier–Stokes equation is presented in the form

$$\mathbf{A}_\beta(x, X, y) = [D_\nu(X)\mathbf{A}_{\alpha_\nu\beta}(X, y)e^{i\int \alpha_\nu(X)\mathrm{d}x} + \varepsilon\mathbf{A}^{(1)}_{\alpha_\nu\beta}(X, y)e^{i\int \alpha_\nu(X)\mathrm{d}x} + \cdots] \tag{8}$$

where $\mathbf{A}_{\alpha_\nu\beta}$ is an eigenfunction satisfying Eq. (5), and function $D_\nu(X)$ has to be determined. The slow function $D_\nu(X)$ in Eq. (8) serves to resolve the uncertainty of $\mathbf{A}_{\alpha_\nu\beta}(X, y)$ normalization. Because coefficients in Eq. (5) depend on the coordinate x, the eigenvalue α_ν is also a slow function of x. Therefore, instead of the phase $\alpha_\nu x$ in Eq. (4), we introduce an integral of $\alpha_\nu(X)$.

After substitution of Eq. (8) into Eq. (1), we arrive at $\mathcal{O}(\varepsilon)$ at an inhomogeneous equation for $\mathbf{A}^{(1)}_{\alpha_\nu\beta}$ with the same leading operator as in Eq. (5), because the terms associated with matrix $\mathbf{H}_4$ have an order of magnitude of $\mathcal{O}(\varepsilon)$. Taking the dot product of the equation with the adjoint solution, $\mathbf{B}_{\alpha_\nu\beta}$, satisfying Eq. (6) and evaluating integral of the result with respect to y from 0 to ∞, we arrive at an ordinary differential equation for D_ν:

$$i\alpha_{\mathrm{np}} = \frac{\mathrm{d}\,\ell n\, D_\nu}{\mathrm{d}x} = -\Gamma^{-1}\left[\left\langle \mathbf{H}_2\frac{\partial \mathbf{A}_{\alpha_\nu\beta}}{\partial x}, \mathbf{B}_{\alpha_\nu\beta}\right\rangle + \langle \mathbf{H}_4\mathbf{A}_{\alpha_\nu\beta}, \mathbf{B}_{\alpha_\nu\beta}\rangle\right] \tag{9}$$

The nonparallel flow effects are represented by two terms in Eq. (9). The first term stems from the slow variation of the eigenfunction with coordinate x and depends on normalization of the eigenfunction. The second term is associated with matrix $\mathbf{H}_4$ that includes the y component of the mean flow velocity and derivatives of the mean flow profiles with respect to the coordinate x. One can see that α_{np} in Eq. (9) is independent of $\mathbf{B}_{\alpha_\nu\beta}$ normalization and depends on normalization of $\mathbf{A}_{\alpha_\nu\beta}$. However, the product $D_\nu(X)\mathbf{A}_{\alpha_\nu\beta}(X, y)$ is invariant with respect to normalization of $\mathbf{A}_{\alpha_\nu\beta}$ (up to a constant complex factor). Thus, the correction factor $D_\nu(X)$ resolves the normalization uncertainty in the case of weakly diverging flow. As a matter of practical application, it is convenient to choose normalization of $\mathbf{A}_{\alpha_\nu\beta}$ in accordance with the quantity of interest. For example, if one is interested in amplitude of the streamwise velocity of the discrete mode, it is convenient to choose normalization of $\mathbf{A}_{\alpha_\nu\beta}$ with $|u|_{\max} = 1$ at all locations x. Then $\sigma = -\mathrm{Im}(\alpha_\nu + \alpha_{\mathrm{np}})$ is the growth rate of $u_{\max}$ in solution (8), in which the nonparallel flow effects are taken into account.

B. Continuous Spectrum

Because eigenfunctions of the continuous spectra oscillate at $y \to \infty$ as $\exp(\pm iky)$, the analysis requires a modification. Instead of a single mode, we consider a narrow-wave packet of width Δk around $k = k_l$. Therefore, solution for the narrow-wave packet is considered in the form

$$\mathbf{A}_\beta(x, X, y) = \left[\int_{k_l-\Delta k/2}^{k_l+\Delta k/2} D_j(X, k)\mathbf{A}_{\alpha_j\beta}(X, y)e^{i\int \alpha_j(X,k)\mathrm{d}x}\mathrm{d}k + \varepsilon\int_{k_l-\Delta k/2}^{k_l+\Delta k/2} \mathbf{A}^{(1)}_{\alpha_j\beta}(X, y)e^{i\int \alpha_j(X,k)\mathrm{d}x}\mathrm{d}k + \cdots\right] \tag{10}$$

where $\mathbf{A}_{\alpha_j\beta}$ is an eigenfunction of the continuous spectra satisfying Eq. (5). We substitute Eq. (10) into Eq. (1) and consider the equation at $\mathcal{O}(\varepsilon)$. Evaluation of the dot product with adjoint eigenfunction $\mathbf{B}_{\alpha_j^l\beta}$ satisfying Eq. (6) at $\alpha_j^l = \alpha_j(k_l)$ and integration of the result with respect to y from 0 to ∞ lead to the ordinary differential equation for D_j as follows:

$$i\alpha_{\mathrm{np}} = \frac{\mathrm{d}\,\ell n\, D_j(X, k_l)}{\mathrm{d}x} = -\Gamma^{-1}\lim_{\Delta k\to 0}\int_{k_l-\Delta k/2}^{k_l+\Delta k/2}\left[\left\langle \mathbf{H}_2\frac{\partial \mathbf{A}_{\alpha_j\beta}}{\partial x}, \mathbf{B}_{\alpha_j^l\beta}\right\rangle + \langle \mathbf{H}_4\mathbf{A}_{\alpha_j\beta}, \mathbf{B}_{\alpha_j^l\beta}\rangle\right]\mathrm{d}k \tag{11}$$

In the limit $\Delta k \to 0$, the integrals in Eq. (11) lead to evaluation of terms such as

$$\int_0^\infty \exp(i(k - k_l)y)\mathrm{d}y = \pi\delta(k - k_l)$$

(see [44]), and the result can be evaluated using asymptotic solutions outside of the boundary layer.

C. Multimode Solution in a Weakly Nonparallel Flow

In the case of a multimode solution, we are presenting our result as

$$\begin{aligned}\mathbf{A}_\beta(x, X, y) &= \sum_\nu D_\nu(X)\mathbf{A}_{\alpha_\nu\beta}(X, y)e^{i\int \alpha_\nu(X)\mathrm{d}x} + \sum_j\int_0^\infty D_j(X, k)\mathbf{A}_{\alpha_j\beta}(X, y)e^{i\int \alpha_j(X,k)\mathrm{d}x}\mathrm{d}k + \mathcal{O}(\varepsilon)\\ D_\nu(0) &= d_\nu\\ D_j(0, k) &= d_j(k)\end{aligned} \tag{12}$$

One should keep in mind that the multimode form of the solution in Eq. (12) admits a mechanism of intermodal exchange due to the weakly nonparallel flow effect. An example of this phenomenon was illustrated by Zhigulev and Fedorov [45], who considered generation of an unstable discrete mode by an acoustic wave. Although the effect is weak when the wave numbers of the modes are different, the exponential amplification of the unstable mode leads to its relatively large amplitude. In the present work, we neglect such intermodal exchange.

The initial values d_ν and d_j in Eq. (12) are to be determined from the receptivity problem solution [18]. In the case of a roughness element, the linearized wall-boundary condition for the streamwise velocity component may be written as follows:

$$y = 0\text{: } u = -f(x, z)U'_w \tag{13}$$

where $U'_w = (\partial U_s/\partial y)_{y=0}$ is the derivative of the unperturbed flow velocity profile. For a localized hump, the nonparallel flow effects on the receptivity problem solution can be neglected in the leading approximation, and one can find [18]

$$\begin{aligned} d_j(k) &= \Lambda\varphi(\alpha_j, \beta), \qquad \Lambda = \frac{U'_w}{\Gamma}[B_{\alpha_j\beta 1}]_{y=0}\\ \varphi(\alpha_j, \beta) &= \int_{-\infty}^{+\infty}\int_{-\infty}^{+\infty} f(x, z)e^{-i\alpha_j x - i\beta z}\mathrm{d}z\mathrm{d}x\end{aligned} \tag{14}$$

where $[B_{\alpha_j\beta 1}]_{y=0}$ is the first component of the adjoint eigenfunction evaluated at the wall.

The nonparallel flow effects may be incorporated into the receptivity problem solution along the lines of the distributed receptivity model proposed by Choudhari [29]. It is shown in [29] that the cumulative effect of distributed wall perturbations can be evaluated using the parallel flow approximation for each piece of the actuator and integrating the result over the distributed actuator. In our case, the result (with the reference point at $x = 0$) will be written as follows:

$$d_j(k) = \int_{-\infty}^{+\infty} \int_{-\infty}^{+\infty} \Lambda(k,x) f(x,z) e^{-i\int_0^x \alpha_j(k,x')\mathrm{d}x' - i\beta z} \mathrm{d}z\mathrm{d}x \quad (15)$$

where $\Lambda(k,x)$ is defined in Eq. (14).

One should keep in mind that the linearized wall-boundary condition equation (13) can be rigorously derived within the triple-deck asymptotic analysis when the height of the hump is small in comparison with the thickness of the viscous sublayer. At finite Reynolds numbers, we do not have criteria for height and length of the hump to specify limits when the linearized boundary conditions can be used. The results should be compared with direct numerical simulations and/or experiments to establish validity of the boundary condition.

IV. Numerical Results

A. Verification: Discrete Mode at $M = 4.5$

For purpose of the developed solver verification, we repeat the results of [36] for a two-dimensional TS wave in a compressible boundary layer over a flat plate at the Mach number 4.5, at the local Reynolds number (based on the Blasius scale) 1550, and at the frequency parameter 130×10^{-6}. The results of [36] were obtained using the method of multiple scales with a slightly different leading operator, when the highest derivatives in coordinate y of the viscous terms in the linearized Navier–Stokes equations were kept in the leading operator, whereas the other viscous terms were treated as perturbations. Figure 1 shows the local growth rate of the mass-flux perturbation as a function of the dimensionless coordinate $\eta = y/\sqrt{\mu_e x/\rho_e U_e}$. Comparison of the mass-flux perturbation corresponding to the discrete mode is shown in Fig. 2.

The method of multiple scales is an asymptotic method that allows taking into account nonparallel flow effects in the leading term. For discrete modes, the method of parabolized stability equations can provide results that are very close to results obtained from the direct numerical simulations (DNS). To illustrate the method of multiple scales used in the present work in comparison with PSE/DNS results [46,47], we consider a discrete mode with the frequency parameter 220×10^{-6}. Figure 3 shows comparisons of results of [46] with the results obtained using the method of multiple scales and using the parallel flow approximation for maximum amplitude in the temperature perturbation. One can see that the leading term of the method of multiple scales provides a good agreement with PSE/DNS results, whereas the parallel flow approximation is inadequate for these conditions. One can also see from Fig. 3 that the nonparallel flow effects are very significant in the example.

B. Roughness Array at $M = 0.02$

In the case of roughness-induced perturbations, there are no discrete modes; only steady normal modes of the continuous spectra represent the perturbation. There are two vorticity modes (A and B), entropy modes, and the acoustic modes (representing Mach waves in the limit $\omega \to 0$) [43].

In the present work, we consider the same array of roughness elements as in [18]. An array of humps is placed at distance x_0 from the leading edge of a flat plate. The geometry of each hump is defined by the function

$$f(x,z) = a\cos^3\left(\frac{\pi\Delta x}{l_x}\right)\cos^3\left(\frac{\pi\Delta z}{l_z}\right) \quad (16)$$

where Δx and Δz are measured from the center of the hump, amplitude $a = 0.172$, $l_x = 27.36$, and $l_z = 22.37$ (in $\sqrt{\mu_e x_0/\rho_e U_e}$ units). The parameters correspond to a hump with a length scale of about 5 times the boundary-layer thickness. Therefore, one may expect that the receptivity of the flow can be analyzed within the quasi-parallel flow approximation. This issue will be addressed later. The local Reynolds number is $Re = 697.37$. The spanwise period of the array is L_z ($2\pi/L_z = 0.073$). In what follows, we include only the first 12 harmonics with $\beta_n = n \times 0.073$.

To evaluate the most significant interval of the parameter k in the present example, in Fig. 4 we show the amplitude factor

$$|\Lambda(k)\varphi(\alpha_j(k),\beta)e^{i\alpha_j(k)(x-x_0)}| \quad (17)$$

for two vorticity modes at $x_* = x - x_0 = 177.3$, $\beta = \beta_1$, and $M = 0.02$. One can see that the main input at these parameters is associated with a k of about 2. We should point out that $\Lambda(k)$ in Eq. (14) is dependent on the eigenfunction normalization. In the case of continuous spectrum, there is not a clear preference for normalization choice. In the problem of interest, the modes of the continuous spectrum are not observable. They just serve as a basis in the eigenfunction expansion, and only their integral has physical meaning. Particularly, the integral leads to zero perturbation outside of the boundary layer, whereas each mode of the continuous spectrum is a function oscillating in y. In the present work, modes of the continuous spectrum are normalized by the wall condition:

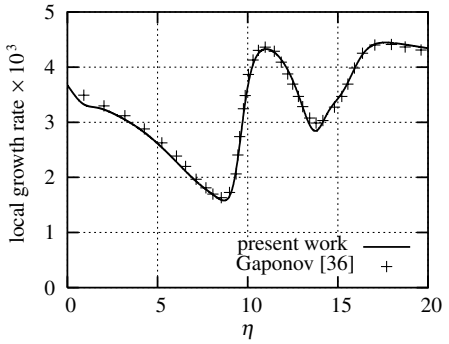

Fig. 1 Local growth rate of the mass-flux perturbation in the boundary layer over a flat plate.

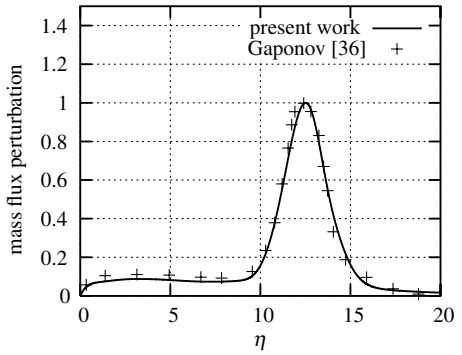

Fig. 2 Mass-flux perturbation in the discrete mode.

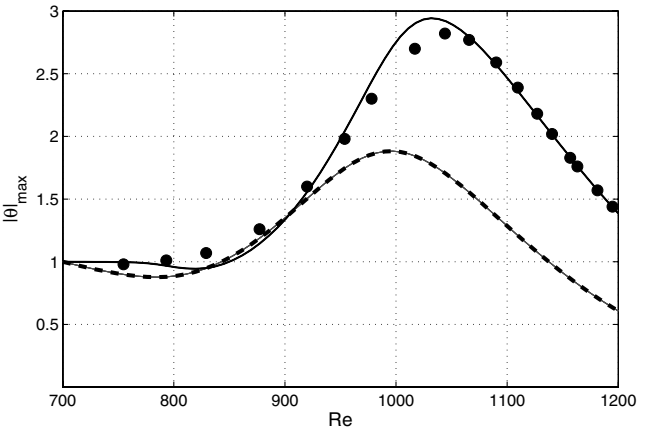

Fig. 3 Amplification of the temperature maximum; method of multiple scales (solid line), parallel flow approximation (dashed line), and PSE (symbols).

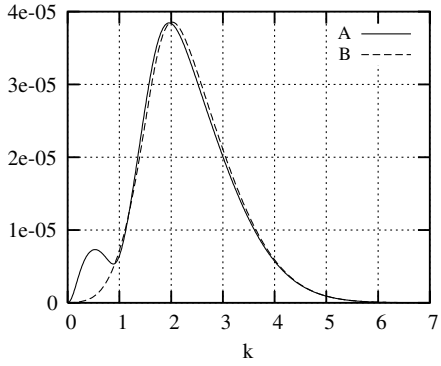

Fig. 4 Amplitude factor [Eq. (17)] at $x_* = 177.3$ and $M = 0.02$ with an adiabatic wall.

$$\left(\frac{\partial u}{\partial y}\right)_{y=0} = 1 \tag{18}$$

Figure 5 shows the variation of normalized $|\Lambda|$ along the roughness element for two vorticity modes at $k = 2$, $\beta = \beta_1$, and $M = 0.02$. The variation of the coefficient is about 1%, and one can consider the receptivity problem within the parallel flow approximation.

Figure 6 illustrates contours of the streamwise velocity perturbation u at $x_* = 177.3$ in the boundary layer at $M = 0.02$ obtained including the nonparallel flow effects and using the vorticity modes only. The continuous spectrum was discretized at $0 \le k \le 5$ using 500 intervals. One can see that there is a wake region downstream from the hump, and there are high-speed streaks on both sides of the hump.

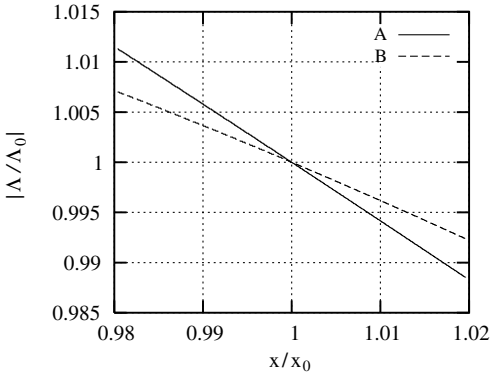

Fig. 5 Variation of normalized $|\Lambda|$ along the roughness element for two vorticity modes at $M = 0.02$ with an adiabatic wall.

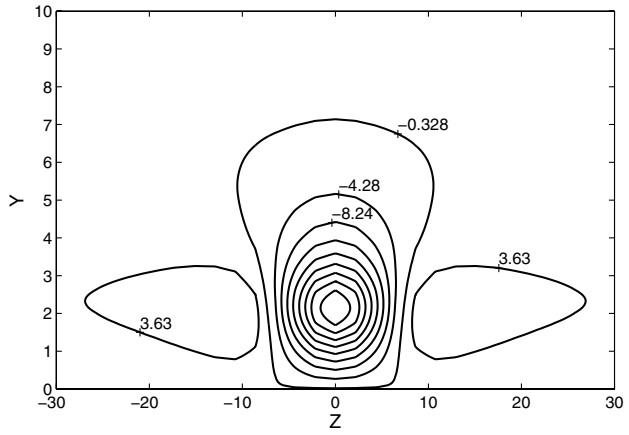

Fig. 6 Contours of $u \times 10^5$ at $x_* = 177.3$ and $M = 0.02$ with an adiabatic wall.

Figure 7 shows the difference between two contour plots: $u_{\text{parallel}} - u_{\text{nonparallel}}$. One can see that the difference is about 10% in the wake.

To understand the source of the difference shown in Fig. 7, we plot real and imaginary parts of the integral

$$N(k) = \int_{x_0}^{x_*} [\alpha(k) + \alpha_{\text{np}}(k, x)]\mathrm{d}x \tag{19}$$

in Fig. 8 for two vorticity modes, together with the result stemming from the parallel flow approximation (in the parallel flow approximation, $N_r = 0$). As discussed in Sec. III, α_{np} depends on the eigenfunction normalization. One can see that the nonparallel flow effects do not have a significant effect on the integral at the chosen normalization. The latter means that the main source of the difference in Fig. 7 is associated with different shapes of the eigenfunctions evaluated at $x = x_0$ (parallel flow model) and at $x = x_0 + x_*$ (nonparallel flow consideration).

Figure 9 shows amplitude distribution of $|u|$ in the boundary layer at $x = x_0$ (lines) and at $x = x_0 + x_*$ (symbols) for $\beta = \beta_1$, $z = 0$, and $k = 1$, 2, and 3. The results illustrate that the difference between the eigenfunctions is greater at lower k. However, amplitudes of eigenfunctions at low k tend to zero (see Fig. 4).

C. Roughness Array at $M = 0.5$

To illustrate the nonparallel effects on the receptivity problem at $M = 0.5$, we present results at the temperature factor $T_w/T_{\text{ad}} = 0.5$ (adiabatic wall was considered in [48]).

Figure 10 shows the amplitude factor defined in Eq. (17) as a function of the parameter k.

Figure 11 shows the variation of normalized $|\Lambda|$ along the roughness element for two vorticity modes and the entropy mode at

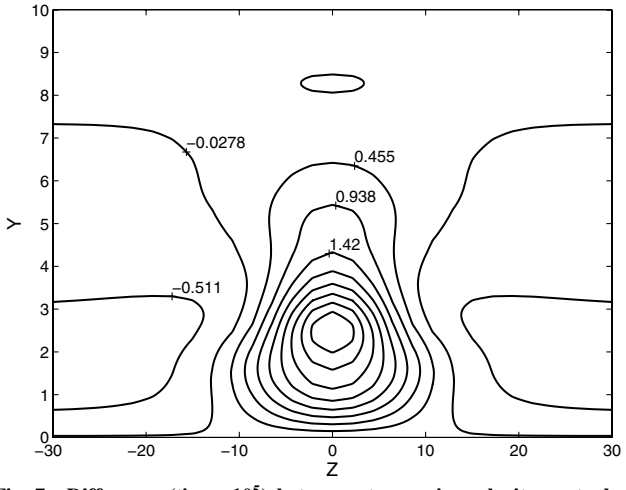

Fig. 7 Difference (times 10^5) between streamwise velocity perturbations obtained within parallel and nonparallel flow models at $M = 0.02$ with an adiabatic wall.

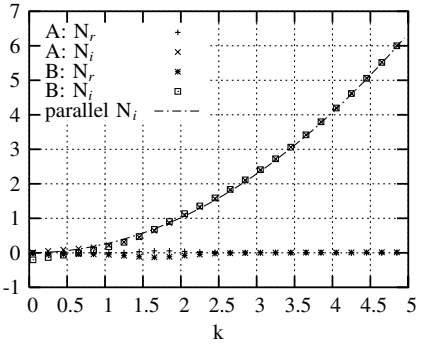

Fig. 8 Integral N for two vorticity modes at $M = 0.02$ with an adiabatic wall.

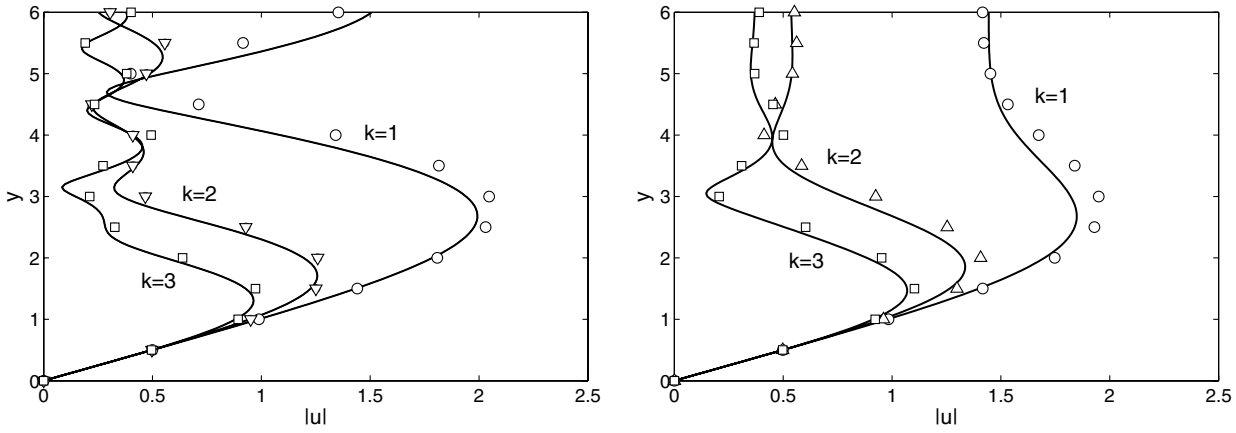

Fig. 9 Distributions of amplitude $|u|$ at $x = x_0$ (lines) and $x = x_0 + x_*$ (symbols) for $k = 1$, 2, and 3 at $M = 0.02$ with an adiabatic wall.: a) vorticity mode A and b) vorticity mode B.

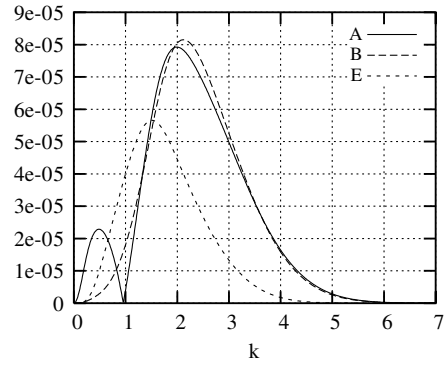

Fig. 10 Amplitude factor [Eq. (17)] at $x_* = 177.3$, $M = 0.5$, and $T_w/T_{ad} = 0.5$; A and B are the two vorticity modes and E is the entropy mode.

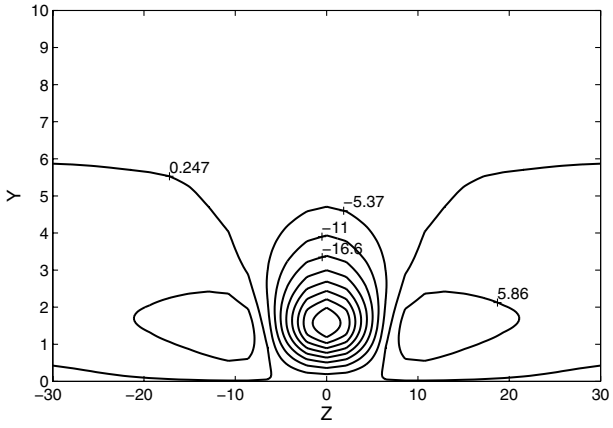

Fig. 12 Contours of $u \times 10^5$ at $x_* = 177.3, M = 0.5$, and $T_w/T_{ad} = 0.5$.

$k = 2$, $\beta = \beta_1$, and $T_w/T_{ad} = 0.5$. The variation of the coefficient is about 1%, and one can consider the receptivity problem within the parallel flow approximation.

Figures 12–15 illustrate the nonparallel flow effect at $M = 0.5$ and the temperature factor 0.5. In these examples, the results were obtained using the vorticity and entropy modes. To avoid overlapping of the vorticity and entropy spectra and to simplify the computations, we use a small nonzero frequency ($\omega = 10^{-5}$), as is described in [43].

Similarly to the example at $M = 0.02$, in Fig. 16 we plot integral N for two vorticity modes and the entropy mode at $M = 0.5$. One can also see that in this case the nonparallel flow effects do not have a significant effect on the integral.

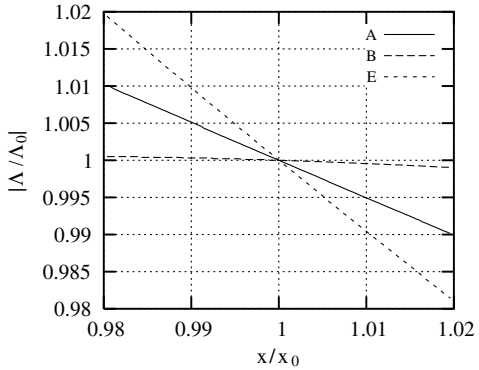

Fig. 11 Variation of normalized $|\Lambda|$ along the roughness at $M = 0.5$ and $T_w/T_{ad} = 0.5$; A and B are the two vorticity modes and E is the entropy mode.

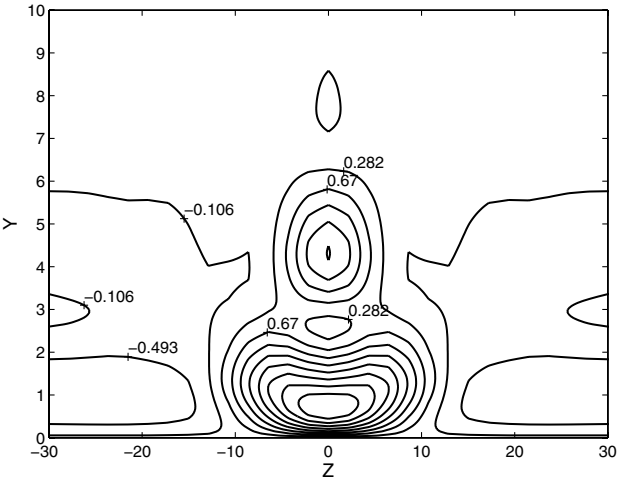

Fig. 13 Difference (times 10^5) between streamwise velocity perturbations obtained within parallel and nonparallel flow models at $M = 0.5$ and $T_w/T_{ad} = 0.5$.

V. Conclusions

To our knowledge, this is the first instance when the weakly nonparallel flow effects are considered for modes of the continuous spectra. The method of multiple scales used in Sec. III is based on separation of characteristic scales for the mean flow and the perturbation. In the case of unsteady perturbations of frequency ω, streamwise wave number of vorticity and entropy modes is $\alpha \approx \omega$, and separation of the scales can be satisfied for $1/\omega \ll x$. In the case

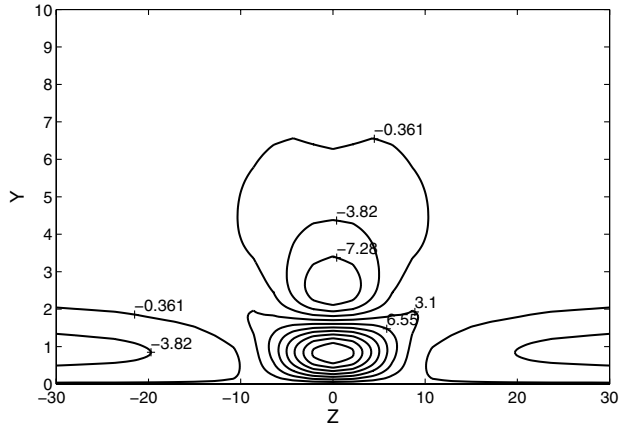

Fig. 14 Contours of $\theta \times 10^5$ at $x_* = 177.3, M = 0.5$, and $T_w/T_{ad} = 0.5$.

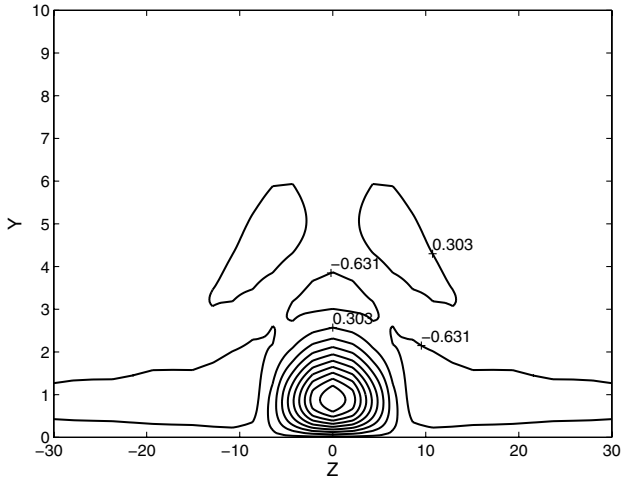

Fig. 15 Difference (times 10^5) between temperature perturbations obtained within parallel and nonparallel flow models at $M = 0.5$ and $T_w/T_{ad} = 0.5$.

of steady perturbations, their characteristic scale is defined by the viscosity effect. At large Reynolds numbers, the decaying rate is about k^2/Re [44], and separation of the scales require $k^2 \gg 1$. The latter means that numerical examples with $k^2 \approx 4$ are marginal, and they should be compared with results of direct numerical simulations to validate the model for steady perturbations.

Although the results obtained with nonparallel flow effects included are quantitatively different from the results obtained within the parallel flow approximation, the qualitative structure of the flowfield downstream of the roughness element remains the same. There is a wake region downstream from the hump, and there are high-speed streaks on both sides of the hump. Temperature increases in the wake region, and there are cold streaks at both sides of the hump. The nonparallel effects lead to a 10% difference in the wake velocity perturbation. Analysis of the nonparallel flow effects in subsonic boundary layers over a flat plate also revealed that one can take them into account just by evaluation of the eigenfunctions at the local Reynolds number downstream from the hump.

In the present work, the nonparallel flow effects on roughness-induced perturbations have been considered for low-speed boundary layers only. The nonparallel flow effects in high-speed boundary layers should be addressed in a future work.

Appendix: Matrix Elements

In what follows, U_s, T_s, and μ_s are streamwise velocity, temperature, and viscosity of the mean flow, respectively, and they are scaled with their values at the edge of the boundary layer; V_s is the vertical velocity of the mean flow; pressure is scaled with $\rho_e U_e^2$; $\mu_s' = d\mu/dT_s$; Re, Pr, and γ stand for the Reynolds number, Prandtl number, and specific heat ratio, respectively; M is the Mach number at the edge of the boundary layer; $D = \partial/\partial y$; parameters r and m are defined as $r = 2(e+2)/3$ and $m = 2(e-1)/3$; and $2e/3$ is the ratio of the bulk viscosity to the dynamic viscosity. Particularly, Stokes's hypothesis corresponds to $e = 0$.

Nonzero elements of the matrices in Eq. (1) are

$$L_0^{43} = -\frac{r\mu_s}{Re}$$

$$L_1^{11} = L_1^{22} = L_1^{33} = L_1^{44} = L_1^{55} = L_1^{66} = L_1^{77} = L_1^{88} = 1$$

$$L_1^{2,10} = L_1^{8,14} = (m+1), \qquad H_1^{12} = 1, \qquad H_1^{21} = -\frac{i\omega Re}{T_s\mu_s}$$

$$H_1^{22} = -\frac{D\mu_s}{\mu_s}, \qquad H_1^{23} = \frac{ReDU_s}{T_s\mu_s}, \qquad H_1^{25} = -\frac{D(\mu_s' DU_s)}{\mu_s}$$

$$H_1^{26} = -\frac{\mu_s' DU_s}{\mu_s}, \qquad H_1^{33} = \frac{DT_s}{T_s}, \qquad H_1^{34} = i\omega\gamma M^2$$

$$H_1^{35} = -\frac{i\omega}{T_s}, \qquad H_1^{43} = i\omega\rho_s, \qquad H_1^{56} = 1$$

$$H_1^{62} = -2(\gamma-1)PrM^2 DU_s, \qquad H_1^{63} = \frac{RePr}{T_s\mu_s} DT_s$$

$$H_1^{64} = i\omega(\gamma-1)\frac{RePr}{\mu_s}M^2$$

$$H_1^{65} = -i\omega\frac{RePr}{T_s\mu_s} - (\gamma-1)\frac{Pr}{\mu_s}M^2\mu_s'\left(\frac{\partial U_s}{\partial y}\right)^2 - \frac{D(\mu_s' DT_s)}{\mu_s}$$

$$H_1^{66} = -\frac{2D\mu_s}{\mu_s} \qquad H_1^{78} = 1, \qquad H_1^{87} = -\frac{i\omega Re}{\mu_s T_s}$$

$$H_1^{88} = -\frac{D\mu_s}{\mu_s}$$

$$H_1^{99} = H_1^{10,10} = H_1^{11,11} = H_1^{12,12} = H_1^{13,13} = H_1^{14,14} = H_1^{15,15} = H_1^{16,16} = -1$$

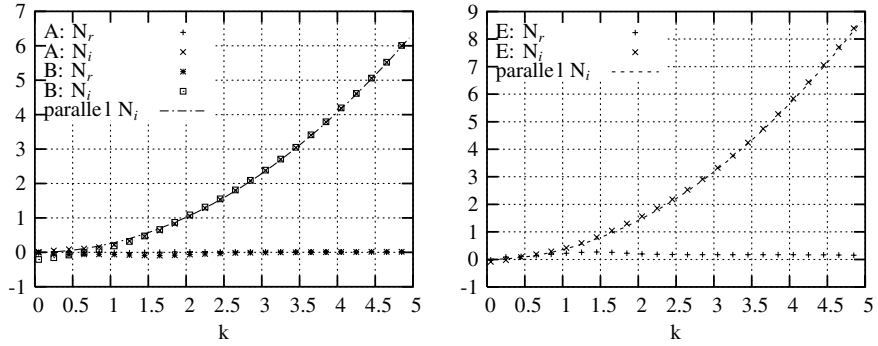

a) **b)**

Fig. 16 Integral N at $M = 0.5$ at $T_w/T_{ad} = 0.5$ for a) two vorticity modes and b) the entropy mode.

$$H_2^{21} = \frac{Re}{T_s \mu_s} U_s, \qquad H_2^{23} = -\frac{D\mu_s}{\mu_s}, \qquad H_2^{24} = \frac{Re}{\mu_s}$$

$$H_2^{29} = -r, \qquad H_2^{31} = -1, \qquad H_2^{34} = -\gamma U_s M^2, \qquad H_2^{35} = \frac{U_s}{T_s}$$

$$H_2^{41} = \frac{mD\mu_s}{Re}, \qquad H_2^{42} = (m+1)\frac{\mu_s}{Re}, \qquad H_2^{43} = -\frac{U_s}{T_s}$$

$$H_2^{45} = \frac{\mu_s'}{Re} DU_s, \qquad H_2^{4,10} = \frac{\mu_s}{Re}$$

$$H_2^{63} = -2(\gamma-1)PrM^2 DU_s, \qquad H_2^{64} = -(\gamma-1)\frac{RePr}{\mu_s} M^2 U_s$$

$$H_2^{65} = \frac{RePr}{T_s \mu_s} U_s, \qquad H_2^{6,11} = -1, \qquad H_2^{87} = \frac{ReU_s}{\mu_s T_s}$$

$$H_2^{8,12} = -1, \qquad H_2^{8,13} = -(m+1)$$

$$H_2^{9,1} = H_2^{10,3} = H_2^{11,5} = H_2^{12,7} = 1$$

$$H_3^{2,12} = -(m+1), \qquad H_3^{2,13} = -1, \qquad H_3^{37} = -1$$

$$H_3^{47} = \frac{mD\mu_s}{Re}, \qquad H_3^{48} = (m+1)\frac{\mu_s}{Re}, \qquad H_3^{4,14} = \frac{\mu_s}{Re}$$

$$H_3^{6,15} = -1, \qquad H_3^{83} = -\frac{D\mu_s}{\mu_s}, \qquad H_3^{84} = \frac{Re}{\mu_s}, \qquad H_3^{8,16} = -r$$

$$H_3^{13,1} = H_3^{14,3} = H_3^{15,5} = H_3^{16,7} = 1$$

$$H_4^{21} = \frac{Re}{\mu_s T_s}\frac{\partial U_s}{\partial x}, \qquad H_4^{22} = \frac{Re}{\mu_s T_s} V_s$$

$$H_4^{24} = \frac{Re}{\mu_s T_s}\gamma M_e^2 \left(U_s \frac{\partial U_s}{\partial x} + V_s \frac{\partial U_s}{\partial y} \right)$$

$$H_4^{25} = -\frac{Re}{\mu_s T_s^2} \left(U_s \frac{\partial U_s}{\partial x} + V_s \frac{\partial U_s}{\partial y} \right)$$

$$H_4^{31} = -T_s \frac{\partial \rho_s}{\partial x} = \frac{1}{T_s}\frac{\partial T_s}{\partial x}$$

$$H_4^{34} = \frac{\gamma U_s M_e^2}{T_s}\frac{\partial T_s}{\partial x} - \gamma M_e^2 \frac{\partial U_s}{\partial x} + V_s \frac{\gamma M_e^2}{T_s}\frac{\partial T_s}{\partial y} - \gamma M_e^2 \frac{\partial V_s}{\partial y} - \gamma M_e^2 V_s \frac{\partial}{\partial y},$$

$$H_4^{35} = -\frac{2U_s}{T_s^2}\frac{\partial T_s}{\partial x} + \frac{1}{T_s}\frac{\partial U_s}{\partial x} - \frac{2V_s}{T_s^2}\frac{\partial T_s}{\partial y} + \frac{1}{T_s}\frac{\partial V_s}{\partial y}, \qquad H_4^{36} = \frac{V_s}{T_s}$$

$$H_4^{43} = -\frac{1}{T_s}\frac{\partial V_s}{\partial y} - \frac{V_s}{T_s}\frac{\partial}{\partial y}$$

$$H_4^{61} = \frac{RePr}{\mu_s T_s}\frac{\partial T_s}{\partial x} - \frac{RePr}{\mu_s}(\gamma-1)M^2 \frac{\partial P_s}{\partial x}$$

$$H_4^{64} = \frac{RePr}{\mu_s}\frac{\gamma M_e^2}{T_s}\left(U_s \frac{\partial T_s}{\partial x} + V_s \frac{\partial T_s}{\partial y} \right) - \frac{RePr}{\mu_s}(\gamma-1)M^2 V_s \frac{\partial}{\partial y}$$

$$H_4^{65} = -\frac{RePr}{\mu_s T_s^2}\left(U_s \frac{\partial T_s}{\partial x} + V_s \frac{\partial T_s}{\partial y} \right), \qquad H_4^{66} = \frac{RePr}{\mu_s T_s} V_s$$

$$H_4^{88} = \frac{V_s}{T_s \mu_s}$$

Acknowledgments

This work was sponsored by the U.S. Air Force Office of Scientific Research under grants FA9550-05-101 and FA9550-08-1-0322 monitored by J. D. Schmisseur. The views and conclusions contained herein are those of the author and should not be interpreted as necessarily representing the official polices or endorsements, either expressed or implied, of the U.S. Air Force Office of Scientific Research or the U.S. Government.

References

[1] Reshotko, E., "Transient Growth: A Factor in Bypass Transition," *Physics of Fluids*, Vol. 13, 2001, pp. 1067–1075. doi:10.1063/1.1358308

[2] Reshotko, E., and Tumin, A., "The Blunt Body Paradox—A Case for Transient Growth," *Laminar-Turbulent Transition*, Springer–Verlag, Berlin, 2000, pp. 403–408.

[3] Tumin, A., and Reshotko, E., "Spatial Theory of Optimal Disturbances in Boundary Layers," *Physics of Fluids*, Vol. 13, No. 7, 2001, pp. 2097–2104. doi:10.1063/1.1378070

[4] Tumin, A., and Reshotko, E., "Optimal Disturbances in Compressible Boundary Layers," *AIAA Journal*, Vol. 41, No. 12, 2003, pp. 2357–2363. doi:10.2514/2.6860

[5] Reshotko, E., and Tumin, A., "Role of Transient Growth in Roughness-Induced Transition," *AIAA Journal*, Vol. 42, No. 4, 2004, pp. 766–770. doi:10.2514/1.9558

[6] White, E. B., "Transient Growth of Stationary Disturbances in a Flat Plate Boundary Layer," *Physics of Fluids*, Vol. 14, No. 12, 2002, pp. 4429–4439. doi:10.1063/1.1521124

[7] White, E. B., and Ergin, F. E., "Receptivity and Transient Growth of Roughness-Induced Disturbances," AIAA Paper 2003-4243, 2003.

[8] Smith, F. T., Sykes, R. I., and Brighton, P. W., "A Two-Dimensional Boundary Layer Encountering a Three-Dimensional Hump," *Journal of Fluid Mechanics*, Vol. 83, 1977, pp. 163–176. doi:10.1017/S0022112077001128

[9] Bogolepov, V. V., and Lipatov, I. I., "Locally Three-Dimensional Laminar Flows," *Journal of Applied Mechanics and Technical Physics*, Vol. 26, No. 1, 1985, pp. 24–31. doi:10.1007/BF00919619

[10] Bogolepov, V. V., "General Arrangement of Regimes for Spatial Local Flows," *Journal of Applied Mechanics and Technical Physics*, Vol. 27, No. 6, 1986, pp. 860–869. doi:10.1007/BF00918829

[11] Bogolepov, V. V., "Perturbations of a Laminar Boundary Layer," *Journal of Applied Mechanics and Technical Physics*, Vol. 28, No. 5, 1987, pp. 706–716. doi:10.1007/BF00912023

[12] Bogolepov, V. V., "Analysis of Flow Regimes in Vicinity of Three-Dimensional Humps," *Transactions of the Central Institute for Aerohydrodynamics (TsAGI)*, Vol. 2376, 1988, pp. 3–29 (in Russian).

[13] Morkovin, M. V., "Critical Evaluation of Transition From Laminar to Turbulent Shear Layers with Emphasis on Hypersonic Traveling Bodies," U.S. Air Force Flight Dynamics Lab., Rept. AFF DL-TR-68-149, Wright–Patterson AFB, OH, 1969.

[14] Reshotko, E., "Boundary-Layer Stability and Transition," *Annual Review of Fluid Mechanics*, Vol. 8, 1976, pp. 311–349. doi:10.1146/annurev.fl.08.010176.001523

[15] Choudhari, M., "Receptivity," *The Handbook of Fluid Dynamics*, edited by R. W. Johnson, CRC Press, Boca Raton, FL, 1998, pp. 13-25–13-40.

[16] Saric, W. S., Reed, H. L., and Kerschen, E. J., "Boundary-Layer Receptivity to Free-Stream Disturbances," *Annual Review of Fluid Mechanics*, Vol. 34, 2002, pp. 291–319. doi:10.1146/annurev.fluid.34.082701.161921

[17] Fedorov, A. V., "Receptivity of a High-Speed Boundary Layer to Acoustic Disturbances," *Journal of Fluid Mechanics*, Vol. 491, 2003, pp. 101–129. doi:10.1017/S0022112003005263

[18] Tumin, A., "Receptivity of Compressible Boundary Layers to Three-Dimensional Wall Perturbations," AIAA Paper 2006-1110, 2006.

[19] Zhigulev, V. N., Sidorenko, N. V., and Tumin, A. M., "Generation of Instability Waves in a Boundary Layer by External Turbulence," *Journal of Applied Mechanics and Technical Physics*, Vol. 21, No. 6, 1980, pp. 774–778. doi:10.1007/BF00912135

[20] Tumin, A. M., and Fedorov, A. V., "Excitation of Unstable Waves in a Boundary Layer on a Vibrating Surface," *Journal of Applied Mechanics and Technical Physics*, Vol. 24, No. 3, 1983, pp. 348–354. doi:10.1007/BF00909752

[21] Tumin, A. M., and Fedorov, A. V., "Spatial Growth of Disturbances in a Compressible Boundary Layer," *Journal of Applied Mechanics and Technical Physics*, Vol. 24, No. 4, 1983, pp. 548–554. doi:10.1007/BF00907906

[22] Tumin, A. M., and Fedorov, A. V., "Instability Wave Excitation by a Localized Vibrator in the Boundary Layer," *Journal of Applied Mechanics and Technical Physics*, Vol. 25, No. 6, 1984, pp. 867–873. doi:10.1007/BF00911661

[23] Fedorov, A. V., "Excitation of Tollmien–Schlichting Waves in a Boundary Layer by Periodic External Source Located on the Body Surface," *Fluid Dynamics*, Vol. 19, No. 6, 1984, pp. 888–893. doi:10.1007/BF01411575

[24] Tumin, A., and Aizatulin, L., "Instability and Receptivity of Laminar Wall Jets," *Theoretical and Computational Fluid Dynamics*, Vol. 9, No. 1, 1997, pp. 33–45. doi:10.1007/s001620050030

[25] Tumin, A., "Biorthogonal Eigenfunction System in the Triple-Deck Limit," *Studies in Applied Mathematics*, Vol. 117, No. 2, 2006, pp. 165–190. doi:10.1111/j.1467-9590.2006.00351.x

[26] Ashpis, D., and Reshotko, E., "The Vibrating Ribbon Problem Revisited," *Journal of Fluid Mechanics*, Vol. 213, 1990, pp. 531–547. doi:10.1017/S0022112090002439

[27] Terent'ev, E. D., "The Linear Problem of a Vibrator in a Subsonic Boundary Layer," *Journal of Applied Mathematics and Mechanics*, Vol. 45, No. 6, 1981, pp. 791–795. doi:10.1016/0021-8928(81)90120-9

[28] Tumin, A., and Reshotko, E., "Receptivity of a Boundary-Layer Flow to a Three-Dimensional Hump at Finite Reynolds Numbers," *Physics of Fluids*, Vol. 17, No. 9, 2005, Paper 094101. doi:10.1063/1.2033907

[29] Choudhari, M., "Distributed Acoustic Receptivity in Laminar Flow Control Configurations," *Physics of Fluids*, Vol. 6, 1994, pp. 489–506. doi:10.1063/1.868345

[30] Bertolotti, F. B., "Receptivity of Three-Dimensional Boundary-Layers to Localized Wall Roughness and Suction," *Physics of Fluids*, Vol. 12, 2000, pp. 1799–1809. doi:10.1063/1.870428

[31] Bouthier, M., "Stabilité Lineairé des Écoulements Presque Paralléles," *Journal de Mécanique*, Vol. 11, No. 4, 1972, pp. 599–621.

[32] Gaster, M., "On the Effects of Boundary Layer Growth on Flow Stability," *Journal of Fluid Mechanics*, Vol. 66, 1974, pp. 465–480. doi:10.1017/S0022112074000310

[33] Saric, W. S., and Nayfeh, A. H., "Nonparallel Stability of Boundary-Layer Flow," *Physics of Fluids*, Vol. 18, No. 8, 1975, pp. 945–950. doi:10.1063/1.861266

[34] Saric, W. S., and Nayfeh, A. H., "Nonparallel Stability of Boundary Layers with Pressure Gradients and Suction," AGARD, TR CP-224, Neuilly-sur-Seine, France 1977.

[35] Padhaye, A. R., and Nayfeh, A. H., "Nonparallel Stability of Three-Dimensional Flows," AIAA Paper 79-1281, 1979.

[36] Gaponov, S. A., "Influence of Nonparallel Flow on the Development of Disturbances in a Supersonic Boundary Layer," *Fluid Dynamics*, Vol. 15, 1980, pp. 195–199. doi:10.1007/BF01342607

[37] Nayfeh, A. H., "Stability of Three-Dimensional Boundary Layers," *AIAA Journal*, Vol. 18, No. 4, 1980, pp. 406–416. doi:10.2514/3.50773

[38] El-Hady, N. M., "On the Stability of Three-Dimensional, Compressible Nonparallel Boundary Layers," AIAA Paper 80-1374, 1980.

[39] Tumin, A. M., and Fedorov, A. V., "On the Weakly Nonparallel Flow Effect on Characteristics of Flow Stability," *Uchenye Zapiski TSAGI*, Vol. 13, No. 6, 1982, pp. 91–96 (in Russian).

[40] Herbert, T., and Bertolotti, F. B., "Stability Analysis of Nonparallel Boundary Layers," *Bulletin of the American Physical Society*, Vol. 32, Nov. 1987, p. 2079.

[41] Bertolotti, F. P., "Linear and Nonlinear Stability of Boundary Layers with Streamwise Varying Properties," Ph.D. Thesis, Ohio State Univ., Columbus, OH, 1991.

[42] Herbert, T., "Parabolized Stability Equations," *Annual Review of Fluid Mechanics*, Vol. 29, 1997, pp. 245–283. doi:10.1146/annurev.fluid.29.1.245

[43] Tumin, A., "Three-Dimensional Spatial Normal Modes in Compressible Boundary Layers," *Journal of Fluid Mechanics*, Vol. 586, 2007, pp. 295–322. doi:10.1017/S002211200700691X

[44] Tumin, A., "Multimode Decomposition of Spatially Growing Perturbations in a Two-Dimensional Boundary Layer," *Physics of Fluids*, Vol. 15, No. 9, 2003, pp. 2525–2540. doi:10.1063/1.1597453

[45] Zhigulev, V. N., and Fedorov, A. V., "Boundary Layer Receptivity to Acoustic Disturbances," *Journal of Applied Mechanics and Technical Physics*, Vol. 28, No. 1, 1987, pp. 28–34. doi:10.1007/BF00918768

[46] Pruett, C. D., and Chang, C. L., "A Comparison of PSE and DNS for High-Speed Boundary-Layer Flows," *Transitional and Turbulent Compressible Flows*, Vol. FED 151, American Society of Mechanical Engineers, New York, 1993, pp. 57–67.

[47] Pruett, C. D., Zang, T. A., Chang, C. L., and Carpenter, M. H., "Spatial Direct Numerical Simulation of High-Speed Boundary-Layer Flows Part 1: Algorithmic Considerations and Validation," *Theoretical and Computational Fluid Dynamics*, Vol. 7, No. 1, 1995, pp. 49–76. doi:10.1007/BF00312399

[48] Tumin, A., "Nonparallel Flow Effects on Roughness-Induced Perturbations in Boundary Layers," AIAA Paper 2008-0504, 2008.

R. Kimmel
Associate Editor